Hybrid lithography fabrication of single mode optics for signal redistribution and coupling

David Weyers, Krszystof Nieweglowski and Karlheinz Bock
Institute of Electronic Packaging Technology
Technical University of Dresden, D-01062 Dresden, Germany
Email: david.weyers@tu-dresden.de

***Abstract*—This paper describes advances in hybrid-lithography process, combining UV-lithography for planar, single mode redistribution layer (RDL) and 2-photon-polymerization direct-laser-writing (2PP-DLW) for micro-mirrors inside RDL-opening. Improvements to multi-layer direct patterning of OrmoCore/-Clad material system using UV-lithography and need for broadband UV-LED source are presented. Near square core cross sections and smooth sidewalls are achieved. Openings in full stack with steep sidewalls without residual layer are patterned. To optimize 2PP-DLW-process processing window for both OrmoComp and IP-DIP is thoroughly characterized. Roughness measurements prove feasibility even of coarsely printed structure as reflective µ-mirror for $1550\,\mathrm{nm}$ wavelength. Finally these results are applied to periscope probe for wafer-level-testing of edge emitting lasers and proof of concept is shown. Outlook to further research on UV-lithography of multi-layer waveguide stack and alignment with µ-mirror printing is given.**

***Keywords*—optical interconnects, single mode, ORMOCER®, hybrid lithography, direct patterning, UV-lithography, 2-photon-polymerization direct-laser-writing, micro-mirrors**

I. Introduction

The ongoing increase in performance and density in high performance computing (HPC) culminating in so-called co-package optics approach where photonic processing units (PPU) or receiver and transmitter (Rx/Tx) are integrated on the same interposer with central processing unit (CPU) and high-bandwidth memory (HBM) is the biggest driver for interposer level optical interconnects and also heavily pushed by industry [1]–[3]. Even more so increasing research and fabrication volume in photonic integrated circuits (PICs) is demanding adequate packaging solutions.

Often butt-coupling to single mode fibers or fiber arrays aligned in v-grooves is used. Whilst this is well established and mechanically stable [4], we believe that it also poses as a limit in integration density and scaling as well as costs, due to the needed chip area for v-grooves, peripheral arrangement on chip/interposer edges and limitation to 1D-arrays. In addition it only provides chip-to-fiber and no chip-to-chip interconnects.

The capability of polymer waveguides (WG) to provide interposer and module level interconnects has been largely demonstrated [5]–[10]. In [11] we proposed a combination of polymer WGs patterned in to an optical RDL via UV-lithography and µ-mirrors structured with 2PP-DLW to provide surface coupling. With the combination of two processes that we termed hybrid lithography we combine the advantages of both. UV-lithography gives parallel, high throughput 2.5D-structuring for the optical RDL. Whilst 2PP-DLW allows for arbitrary 3D-shaped µ-mirrors changing both optical axis and beam shape. This allows for a higher IO-count and integration density compared to fiber butt-coupling. The so-called optical back end of line (BEOL) shown in Fig. 1 can be added to an existing electrical interposer to add optical function.

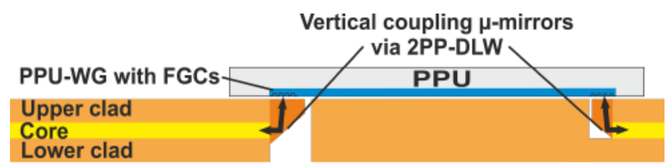

Figure 1. Schematic of the optical BEOL consisting of polymeric RDL with vertical coupling micro-mirrors used to connect to a PPU with integrated WGs and FGCs.

This paper details our recent advances in the hybrid lithography process. The processing section will begin with a brief description of the flow. We demonstrate that bottom cladding can be used to planarize topography from metal RDL and pads forming the electrical interconnects on the interposer. Thereafter measures taken to improve the UV-lithographic patterning, with the final one being the upgrade to a new UV-LED source, will be described. The second part of processing will detail a method used for semi automated resin characterization and comparison for the 2PP-DLW process. This will then be applied to a periscope probe for wafer level testing of edge emitting lasers. Thereafter we will characterize UV-lithographic patterning results using scanning electron microscopy (SEM) and explain why the UV-LED source is necessary for reproducible patterning. We will present the 2PP-DLW process window for IP-DIP resin and conclude its suitability for our application. SEM images of the printed structures will be undermined with tactile profilometry measurements to prove that even a visible roughness in SEM can be well below $\lambda/10$. Thereafter printing results of the periscope probe and its application in the measurement of edge emitting lasers are shown. Finally we conclude our work and provide an outlook to future research.

II. PROCESSING

We previously demonstrated light transmission across two µ-mirrors and a WG inside the optical BEOL [12]. However patterning quality was not ideal, thus this chapter will focus on upgrades to the individual steps of hybrid lithography process to improve structure quality, thus bare silicon is used as a substrate. Fig. 2 gives an overview on the full process flow to transform an electrical Si-interposer into an hybrid. Second focus will be on ensuring that all process development is compatible to the Si-interposer substrate.

A. UV-Lithography

In [10]–[12] we improved our UV-lithographic direct patterning of WGs from multi to single mode dimensions. With the reduction in layer height and feature size the formation of an inhibition layer of $5\,\mu m$ with the used ORMOCER®-material system demanded inert atmosphere during exposure. Additionally it has to be exposed with a proximity gap, since it is sticky after spin-coating.
Previously we set the proximity gap by referencing contact of wafer and mask before coating the layer, however the used mask aligner EVG640 does not allow for reproducible setting of low proximity gap. Since the resin is still sticky after pre-bake the mask will be fully wetted even from a small contact. To ensure a low and reproducible gap we structure SU8 spacers around the wafer edge. First the substrate is spin cleaned with acetone und isopropanol, thereafter SU8-3025 is coated at $1500\,\mathrm{RPM}$ and soft baked for $15\,\mathrm{min}$ at $95\,°\mathrm{C}$. Since resolution is uncritical for spacers a foil mask and contact exposure with $400\,\mathrm{mJ\,cm^{-2}}$ at $365\,\mathrm{nm}$ (i-line) is used to structure $1\,\mathrm{mm}$ long and $400\,\mu m$ wide, triangular spacers that are $2\,\mathrm{mm}$ from wafer edge and pointing inwards. Post exposure bake is carried out for $1\,\mathrm{min}$ at $65\,°\mathrm{C}$ and $5\,\mathrm{min}$ at $95\,°\mathrm{C}$ before the spacers are developed for $10\,\mathrm{min}$ in Mr-Dev600 and rinsed with IPA. Any residues of SU8 will later cause holes in the BEOL, thus full development of the layer must be achieved. Spacers are fully inside the edge bead and thus the height of $90\,\mu m$ is much higher then data sheet value of $40\,\mu m$. They are high enough to be used for the full $50\,\mu m$ optical BEOL and accompany for some wafer bow and thickness non uniformity but still small enough to allow patterning of the $7\,\mu m$ WG-cores.
To achieve a numerical aperture (NA) of 0.14, matched to typical single mode fiber (SMF), a mixture of 70% OrmoCore and 30% OrmoClad is used as bottom and top cladding and will be referred to as OrmoCladXP. By ordering this premixed in syringes directly from micro resist technology, we were both able to solve problems with small bubbles after spin coating and achieve good control over applied amount of resin by using a pneumatic dispenser. Before applying the resin O_2-plasma activation is performed for best adhesion [11]. Undiluted resin and a spin speed of $3000\,\mathrm{RPM}$ yielding a thickness of $27\,\mu m$ was derived from planarization tests on $6\,\mu m$ topography from pads and RDL on Si-interposer, that will be explained later in the characterization chapter. edge beat removal (EBR) is performed by spraying OrmoThin onto the wafer edge during the last $10\,\mathrm{s}$ of spin coating. This removes most of the resin from the spacers, small amounts might touch the mask, but the wafer can not be pulled towards the mask due to the spacers. Since the mask is opaque at the wafer edge, those residues will not be exposed and can be easily washed away using the development process. Thirdly pre-bake for $4\,\mathrm{min}$ at $85\,°\mathrm{C}$ is carried out. Even though this is only necessary for thinned resin to evaporate OrmoThin, we see improvement to layer uniformity during the pre-bake. At forth exposure is performed. To ensure a good N_2-atmosphere and thus reduce inhibition we use a custom chuck with N_2-inlets surrounding the wafer and rinse for $2\,\mathrm{min}$ with $400\,\mu m$ separation before bringing spacers into contact with the mask. Exposure is then performed in this quasi-contact-mode, initially with a i-line Hg-lamp. Puddle development in spin coater is used. Sample is exposed to OrmoDev for $30\,\mathrm{seconds}$ and spin cleaned twice with OrmoDev and once with IPA. Those steps are then repeated for core and top cladding. $3\,\mathrm{mL}$ of OrmoCore diluted 4:1 with OrmoThin are pipetted for the core layer to yield a thickness of $7\,\mu m$ at $3000\,\mathrm{RPM}$. After printing the µ-mirrors using 2PP-DLW, full exposure with $1000\,\mathrm{mJ\,cm^{-2}}$ to deplete residual iniator and a $3\,\mathrm{h}$ hard bake with $30\,\mathrm{min}$ up-ramp is carried out to improve stability and

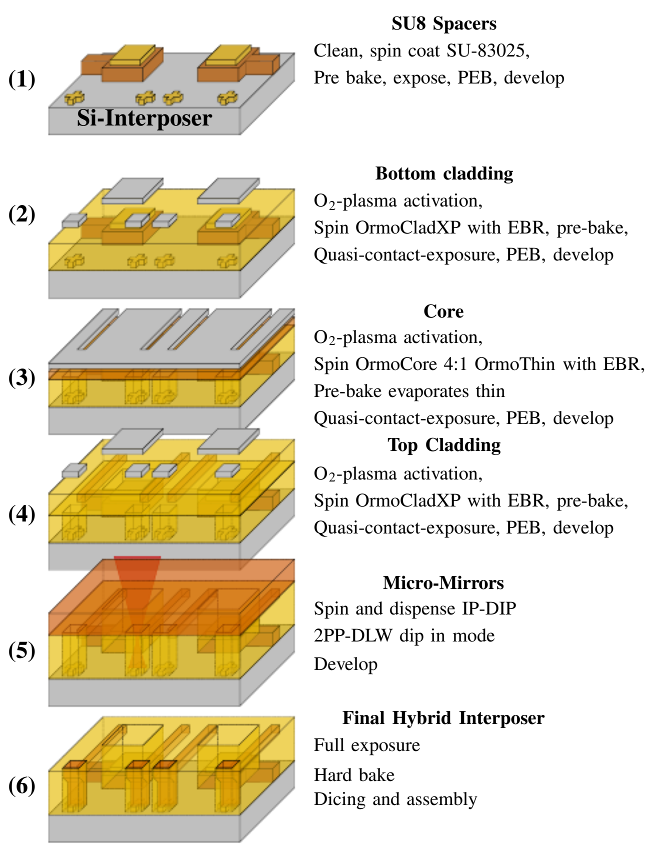

Figure 2. Schematic hybrid lithography process flow for polymeric optical BEOL on Si-interposer with Cu-RDL, passivation and pads.

adhesion.
Main focus of the process development is to improve patterning quality by working on the exposure. In [12] we explained, that our i-line Hg-lamp non-ideal, since it has to be moved away from its dedicated operation point to reduce lamp power, so that needed doses of a few $\mathrm{mJ\,cm^{-2}}$ can be delivered at reliable shutter times $> 0.8\,\mathrm{s}$. Nevertheless we tried to improve the patterning both by the spacers and using optical proximity structures (OPC) patterns in the mask. To further improve patterning we upgraded to a UV-LED exposure source with two broadband spectra at $365\,\mathrm{nm}$ (i-line) and $405\,\mathrm{nm}$ (h-line), separately tunable in power, and pulse time as short as $100\,\mathrm{ms}$ and up to $65\,\mathrm{mW\,cm^{-2}}$, allowing for short, high power exposure to further reduce inhibition. Patterning results for bottom cladding and core with the two setups and different doses will be compared in the characterization section.

B. Micro-Mirror Fabrication

The 2PP-DLW-process is based on two-photon-absorption (TPA) of negative tone resins inside the focal volume, so-called voxel (volumetric pixel) of a highly focused $780\,\mathrm{nm}$ laser. Regular single photon absorption is proportional to intensity whereas TPA is to intensity square, thus resin contrast is much larger and voxel can be tuned down 300-$400\,\mathrm{nm}$ diameter and 800-$1000\,\mathrm{nm}$ height [13], [14]. Laser beam is moved along a 3D-trajectory with the overlapping voxels forming an arbitrary 3D-structure. This capability makes it an ideal process for µ-mirrors.
Nanoscribe photonic GT2 machine is used for printing the µ-mirrors. A resin droplet is dispensed onto the substrate, for larger substrates a thin layer has to be spin coated in addition. Since the substrate is opaque we use so called dip-in mode, where the objective is then moved into the droplet. The surface is referenced by its reflection, thus only the interface between substrate and polymeric BEOL can be found, since all other interfaces have low refractive index step and thus reflection. This makes good process stability in lithography critical so that the mirrors can be accurately placed in front of WG-cores in z-direction. Since the linear stage used to move laterally across the wafer is only accurate to a few µm, local alignment marks in the pad layer are used for every mirror. They can be referenced using the in-line camera, however only with the 63x objective resolution is high enough for sub-µm alignment. Therefore we use it, even though 25x would allow for faster printing with still sufficient resolution for our $20\,\mathrm{µm}$ wide mirrors. To form the structure the beam is steered in concentric trajectories in plane using a galvanic mirror system and the planes are stacked by moving the sample away from the objective with a piezo. In-plane trajectory distance is called hatch (H) and plane distance slice (S). Together with laser power and scan speed those are the most important process parameters. After printing the objective is moved out of the droplet and sample is developed in PGMEA bath for $10\,\mathrm{min}$ and rinsed in isopropanol for $2\,\mathrm{min}$. Since this is a well established process our focus is on reducing processing time and variation without degrading structure and thus optical quality. In [15] we achieved good results with OrmoComp resin, which is related to used WG material system. However OrmoComp has a strong tendency to overexposure causing the structures to look inflated, which causes additional lens effects. Thus we present a comparison to IP-DIP resin in this paper. Since the path of beam through the mirror is very short, small differences in absorption only have a minor impact, thus the patterning conformity, process stability and mechanical stability are the most important aspects. To ensure the later, adhesion tests similar to those for optical RDL in [11] were carried out on the contact interfaces of the µ-mirrors: Si, SiO_2 and bottom clad. For characterizing the processing window a large matrix of identical structures with different hatch and slice, scan speed and laser power was printed. Since we are aiming at roughly $45°$ mirrors identical hatch and slice from 100-$700\,\mathrm{nm}$ was used. All structures were lifted on a $15\,\mathrm{µm}$-high coarse written base to get away from the silicon reflection, which alters power density. Laser power was varied in 7 levels between $6.5\,\mathrm{mW}$ and the maximum of $65\,\mathrm{mW}$. Maximum scan speed of the machine is $200\,\mathrm{mm\,s^{-1}}$. Minimum scan speed for each combination of laser power, hatch and slice was set using the equation 1 and at least to $100\,\mathrm{µm\,s^{-1}}$, below the line starts to wobble [11]. Logarithmic sweep with 10 values per decade and at least 2 decades is applied.

$$SS_{min} = 0.1 * \frac{(P/[\mathrm{mW}])^2}{h/[\mathrm{µm}] * s/[\mathrm{µm}]} \tag{1}$$

Characterization of these samples will be presented later in the respective section. For roughness characterization $40\,\mathrm{µm}$ wide, $50\,\mathrm{µm}$ high trapezoid structures with $50\,\mathrm{µm}$ long, $45°$ up and down ramp are printed. All parameter sets within processing window that allow for feasible printing time are used. To ensure compatibility of µ-mirrors to proposed interposer adhesion tests as for polymeric RDL in [11] were carried out. Pillars of IP-DIP with $50\,\mathrm{µm}$ diameter and $20\,\mathrm{µm}$ were printed on Si, SiO_2 and OrmoCladXP. For printing on substrate materials coarse parameters as for bases in process window experiment and on OrmoCladXP fine mirror parameters were used. For substrate materials tested adhesion treatments were: none, dehydration bake for $5\,\mathrm{min}$ at $200\,°\mathrm{C}$, oxygen plasma, OrmoPrime and silanization. Finally results were already applied to so called periscope probe in Fig. 3.
A project partner in VE-Silhouette presented us with the challenge of probing edge emitting lasers on wafer level. Since the facet is inside a small trench periscope probe was proposed. Centerpiece are the vertical and horizontal WGs connected via µ-mirrors, coupling emission from the laser to a multi mode fiber placed underneath the support structure. Probe tip is extending $60\,\mathrm{µm}$ above, thus can be lowered into the laser's trench without touching the substrate surface. It is tilted so the tip can be found when looking through the assembly under prober microscope.

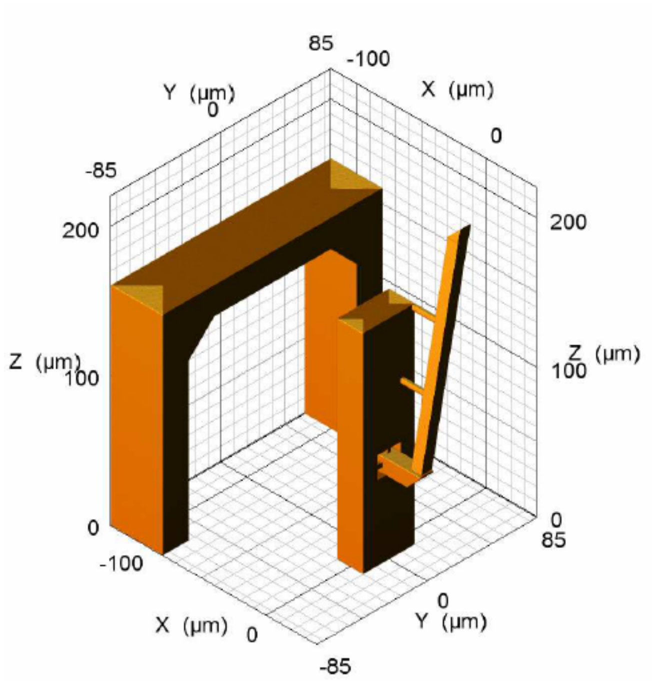

Figure 3. Design of the periscope probe with tilted $8\,\mu m$ square WG with mirror on top, coupling into $10\,\mu m$ horizontal WG via mirror. Horizontal WG height is set to match multi mode fiber core held with support structure. WGs are held with $2\,\mu m$ studs.

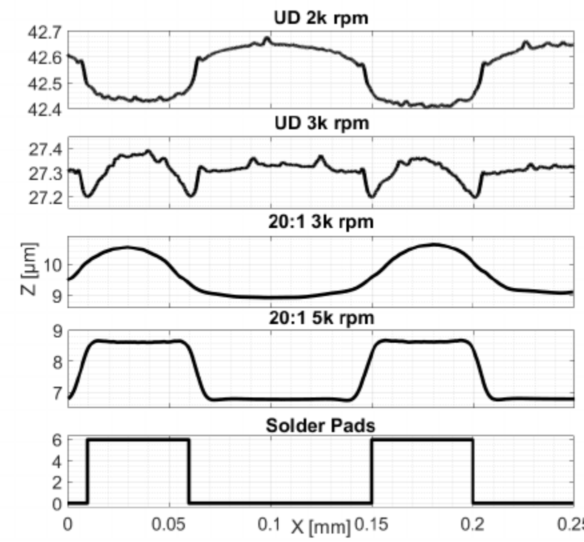

Figure 4. Surface profile measured using tactile profilometry of bottom clad on $6\,\mu m$ solder pad topography pretreated with oxygen plasma. Undiluted (UD) OrmoCladXP and dilution 20:1 with OrmoThin at different spin speeds are compared. Best planarization is achieved for undiluted OrmoCladXP spun on at $3000\,RPM$.

Laser is emitting at short visible wavelength, thus hatch and slice of $100\,nm$ with laser power and scan speed at $20\,mW$ and $10\,mm$ were used for the light path. This gives very low roughness and corner rounding with acceptable process time. For the support structures hatch and slice of $200\,nm$ with laser power and scan speed at $30\,mW$ and $20\,mm$ were used to decrease processing time but still give a transparent structure, so it does not obscure tip. This leads to a print time of $30\,min$. Print is placed roughly $200\,\mu m$ from edge of $5\,mm$ by $25\,mm$ fused silica substrate, again so that the diced substrate edge does not obscure tip. Fused silica is used since it is transparent and refractive index is low enough to reference interface to IP-DIP resin. After printing the substrate is glued into an stereo lithographically printed base allowing for mechanical fixation to probe manipulators and the fiber. A $50\,\mu m$ core, 0.2 NA fiber is stripped at its end and cleaved. The fiber facet is carefully maneuvered under the support structure and in front of horizontal WG facet. It is then glued to both the substrate and base.

III. Characterization

In this section we characterize produced samples both geometrically and optically. We highlight and explain deviations as well as possible solutions.

A. Optical RDL

For fast process development Optical RDL test samples are first characterized using optical microscopy, tactile profilometry and SEM imaging. Only if process parameters are deemed, feasible functional WGs are manufactured and optically tested. For the polymeric RDL to function on a Si-interposer bottom clad has to planarize topography from $6\,\mu m$ solder pads so that WG-cores do not get extra loss from roughness, waviness and z-position is accurately aligned to µ-mirrors. Different dilutions and spin speeds were tested with OrmoCladXP on Si-interposer samples treated with either oxygen plasma or OrmoPrime. After spin coating bottom clad was fully exposed and topography was measured using tactile profilomety. OrmoPrime lead to extended waviness above pads, needing bottom clad thickness exceeding $50\,\mu m$, that can no longer be bridged by the electrical interconnect. Fig. 4 shows selected results for oxygen plasma. With increasing layer thickness sharp pad topography gets smoothed out, until at $27\,\mu m$ only $\pm 100\,nm$ topography from pad and edge is left and the section between pads, where WG-cores will be in functional layout, is flat with roughness below $\lambda/10$.

With the introduction of SU8 spacers we achieved a lower proximity gap yielding close to square core cross sections in Fig. 5 with improved end facets, compared to what we reported in [11]. Additionally $0.5\,\mu m$ wide scattering bars in the mask present for all but the right most WG give a more perpendicular side wall. Best result is achieved for second right with lowest distance between scattering bar and WG mask opening. However root like structures are still clearly visible, even though extend is reduced by lower proximity gap. Additionally sidewalls have rough, standing wave pattern in Fig. 6a and correct exposure dose is only found for parts of wafer due to big inhomogeneity. Thus WGs with fine $32\,\mu m$ pitch showed losses above $1.5\,dB\,cm^{-1}$, exceeding what we reported in [11], and strong cross coupling shown in Fig. 7.

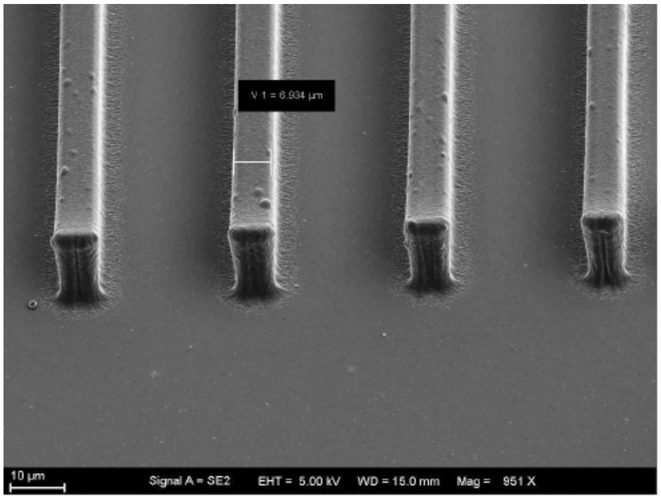

Figure 5. Dimetric SEM-image of WG cores processed with Hg-lamp and SU8-spacers. right most has no scattering bar, others have 0.5 µm bar with increasing distance to mask opening. Square cross section but root structures and rough sidewalls.

Similarly for the clad openings we were able to improve structure quality shown in Fig. 6c, however we could not achieve open bottom with full layer thickness for 20 µm openings. OPC structures only improved the hole shape but not sidewall angle or residual layer at the bottom.

Thus we concluded that our setup with Hg-lamp moved out of dedicated working point is not feasible, mainly due to bad parallelization of light and standing wave effects. However with the recent upgrade to dual wavelength UV-LED source we were able to achieve core cross section in Fig. 6b and clad opening in Fig. 6d. Core has smooth sidewalls and

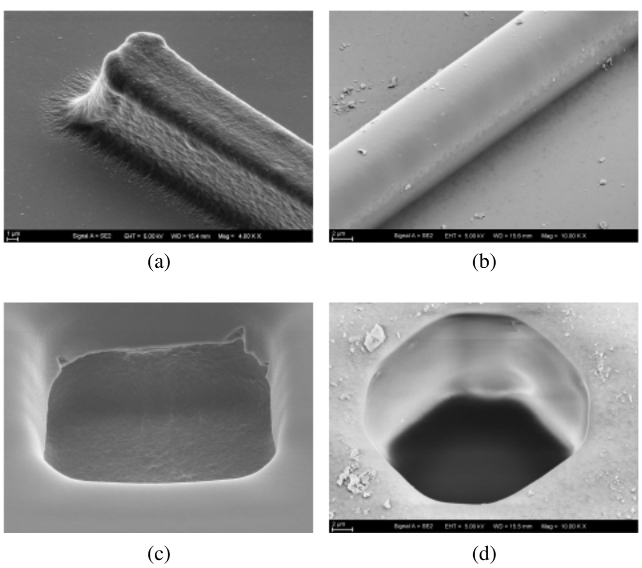

Figure 6. Best results for WG-cores (top) and clad openings (bottom) patterned with Hg-lamp (left), 365 nm and 405 nm dual wavelength UV-LED source (right).

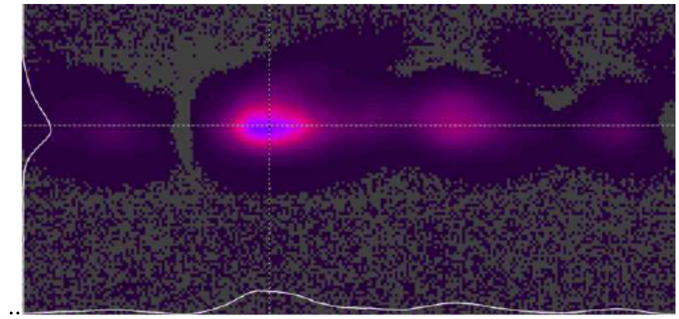

Figure 7. Power distribution at output facet of 4 WGs with 32 µm-pitch and light only being coupled into the second from left, measured using InGaAs beamprofiler showing strong cross coupling.

top without root like structure. We attribute this to the dual wavelength source preventing standing wave effects and much more parallel light source. Attenuation and cross coupling are yet to be measured but expected to be improved. Exposure result is uniform across wafer and identical for 32 µm and 64 µm pitch. Similarly sidewall of opening in Fig. 6d is steeper and smooth, there is no residual layer at the bottom and full layer thickness of 27 µm is achieved.

B. Micro-Mirrors

To characterize processing of different resins with 2PP-DLW more than 1000 structures per resin and optic we're printed. Due to serial nature of the process this can be done in a single run. To extract full information from those parameter sweeps and not just find one working process point, automatic characterization method had to be developed. Therefore we automatically took isometric images of every structure using SEM. Every parameter set could then be graded qualitatively in 8 different ranks shown in Fig. 8.

Since absorption is proportional to intensity square it can be so high that resin evaporates locally and forms a bubble, if this is the case all along the structure it ends up being defect as in Fig. 8a. If this is only reached due to lower printing speed when changing direction in corners or at a particle in resin a bubble only takes up part of the structure as in Fig. 8b. If dose is decreased but still too high the structure appears inflated in Fig. 8c giving a certain deviation from the designed shape. Goal is to produce a smooth, according to design structure, as in Fig. 8d. As the dose is further decreased, voxel overlap reduces and thus the individual lines can be distinguished under SEM in Fig. 8e, impact on structure roughness will be detailed later. Further decrease in dose makes the structure shrink (fig. 8f) and become unstable (fig. 8g). In addition low dose corresponds to high printing speed, for used structure size only speeds up to roughly $40\,\mathrm{mm\,s^{-1}}$ can be used, above corner deviation dominates as shown in Fig. 8g. If power inside voxel is below absorption threshold no structure is formed (fig. 8h).

Comparing the results in Fig. 9 gives different tendency of resins. While Ormocomp shows no bubbling, it has strong overexposure and processing window is thin but ranges across

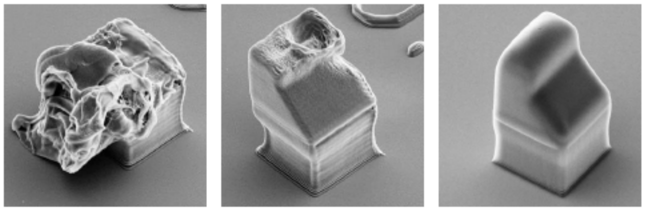

(a) Defect structure (b) Bubbles in structure (c) Overexposed

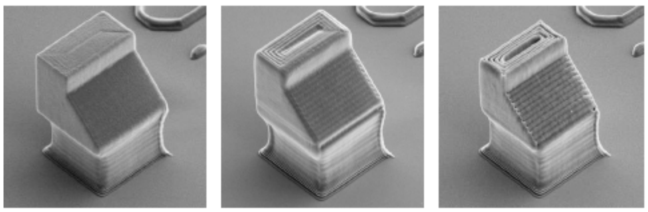

(d) Smooth (e) Visible roughness (f) Underexposed

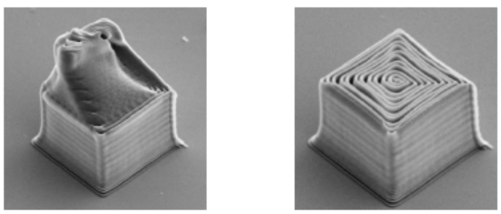

(g) Small/collapsed (h) No structure

Figure 8. Typical structures for each qualitative grade used to define processing window and compare resins. Exposure dose decreases from (a) to (h). Usable process window from (c) to (f), however ideally only (d) and (e) if roughness is below λ/10 are used.

most powers. In comparison IP-DIP shows strong bubbling but low tendency to overexposure. Goal is to produce a structure with below $\lambda/10$ roughness, low shape deviation and processing time. From a time standpoint hatch and slice should be chosen as high as feasible. Since printing speed is reduced during direction change in corner, time is not directly proportional to printing speed and a sweet spot is roughly at $10\,\mathrm{mm\,s^{-1}}$. In addition process variation mainly from resin temperature and aging as well as laser power variation and drifting must be taken into account. Thus it is preferable to use a parameter set in the middle of a bigger processing window. IP-DIP meets these criteria for both hatch and slice of $0.2\,\mu\mathrm{m}$ and $0.3\,\mu\mathrm{m}$ and was thus used for further experiments. However within this processing window structure quality changes from smooth to visible roughness. For further investigation tactile profilometry with $8.3\,\mathrm{nm}$ lateral and $0.1\,\mathrm{nm}$ vertical resolution using $50\,\mathrm{nm}$ tip radius stylus was carried out. Since the structure is only $140\,\mu\mathrm{m}$ long, 30 parallel lines are measured to increase data points.

For roughness characterization on 3D structures filters are used to separate profile and roughness. For the used structures a cut-off of $1\,\mu\mathrm{m}$ should be used, however this would also partially filter roughness signal from voxel lines with $500\,\mathrm{nm}$ hatch. Thus each line was separated into 3 segments up, top and down and linearly flattened. For all samples a waviness

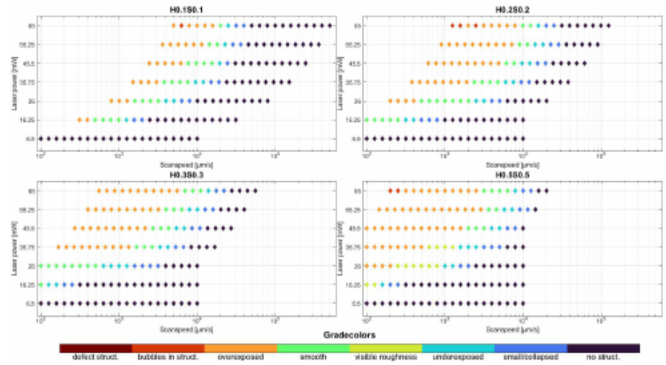

(a)

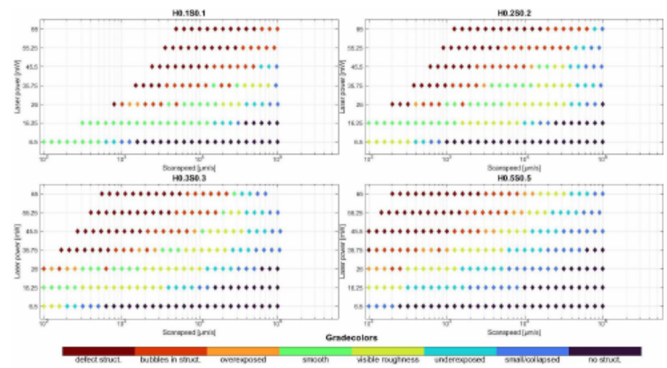

(b)

Figure 9. Process window graph for resins OrmoComp (a) and IP-DIP (b) showing bigger usable process window for IP-DIP and small overexposure effect, but higher tendency to form bubbles. OrmoComp however has strong overexposure causing structures to appear inflated with higher dose.

with 5-10 $\mu\mathrm{m}$ period and up to $1\,\mu\mathrm{m}$ amplitude was observed. This should be visible in iso- and dimetric view under SEM, but is not. Thus is likely introduced by the measurement system. To further investigate spatial line scan data was transferred to a periodic spectral density (PSD) graph using Welch's method. Fig. 10 shows this for coarse hatch and slice

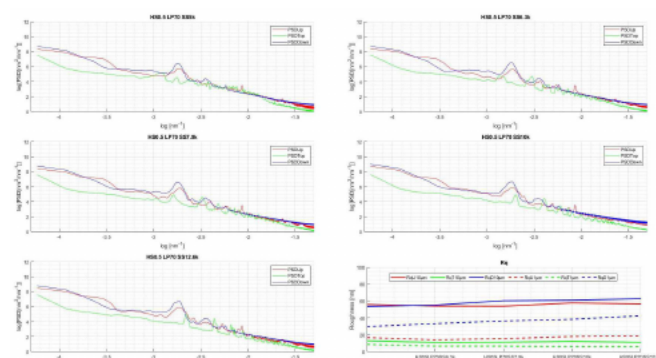

Figure 10. PSD-graph from tactile profilometry with $8.3\,\mathrm{nm}$ lateral and $0.1\,\mathrm{nm}$ vertical resolution using $50\,\mathrm{nm}$ tip radius stylus. Peak from $500\,\mathrm{nm}$ hatch is increasing with scan speed, since lower dose decreases voxel size and thus separation. However roughness in bottom right graph is still below λ/10 and only mildly increasing.

of $500\,\mathrm{nm}$. For all scan speeds the peak corresponding to hatch is clearly distinguishable and is increasing in height with scan speed, since voxel outlines are becoming more separated. This is stronger in up and down ramp, since here scan direction is always perpendicular to print trajectory however on top it is mostly parallel. For lower length scale all three segments give similar reads in PSD-graph. In contrast for higher length scale of few $\mu\mathrm{m}$ there is a gap of two decades in spectral density between the two graphs, given by the previously explained measurement error. This leads to the fact that R_q with $10\,\mu\mathrm{m}$ cut-off, given by the solid lines, is only minor higher then for $1\,\mu\mathrm{m}$ cut-off for the top section but much higher for the sloped sides. We conclude from that, that the $1\,\mu\mathrm{m}$ cut-off can be used. As shown in the R_q-graph it is higher for the slopes and slightly increasing due to the increase of voxel separation. However it has to be noted, that even for coarse printing it is still below $\lambda/10$ and thus still feasible as μ-mirror.

For lower hatch the increase in roughness suggested by transition from smooth to visible roughness in Fig. 9b could not be measured. Within the processing window R_q is between $10\text{-}15\,\mathrm{nm}$ for hatch of $100\,\mathrm{nm}$ and $200\,\mathrm{nm}$ and increases to around $20\,\mathrm{nm}$ for $300\,\mathrm{nm}$ hatch.

Functional feasibility for μ-mirrors is shown, for compatibility to hybrid interposer adhesion tests were performed. Each pair of surface treatment and substrate 20 pillars were sheared before and after thermal treatment. Adhesion for both Si and SiO_2 was by far the best with OrmoPrime in the $30\text{-}40\,\mathrm{MPa}$ range and with only minor impact of thermal treatment up to $300\,^\circ\mathrm{C}$, simulating reflow soldering. All other treatments yielded inferior adhesion that was dropped to below $5\,\mathrm{MPa}$ already by thermal treatment with $270\,^\circ\mathrm{C}$. For OrmoCladXP no pretreatment was compared only to oxygen plasma and bake. Here no pretreatment yielded the best adhesion of arround $40\,\mathrm{MPa}$ and is stable with temperature exposure.

Since the mirror has large contact area to OrmoCladXP in opening of polymeric RDL, low adhesion to substrate should not present a problem. Since OrmoPrime is made to bond acrylates to inorganic substrates it can not be used on OrmoCladXP. The only way would be to use it for polymeric RDL already, were it yielded similar adhesion as oxygen plasma [11]. However it performed worse in planarization tests and it's unclear whether it would still be present on substrate surface after polymeric RDL processing.

As one application of μ-mirrors periscope probe was tested with edge emitting laser still on wafer. Fig.11a shows that the goal of a transparent assembly allowing for coarse placement of the probe to laser facet was met. In addition assembly is small enough so that it does not block the DC-probes supplying laser with current. This is to our knowledge the first demonstration of such a setup, previously similar probes were printed on fiber tip, however here the fiber obscures tip view [16]. During testing this assembly automatic manipulation with sub-μm resolution as for testing of optical RDL is necessary to find maximum coupling without crashing the fiber into trench bottom. Fig. 11b shows the tip after crashing it. However with this tip we were still able to measure $600\,\mu\mathrm{W}$ from laser

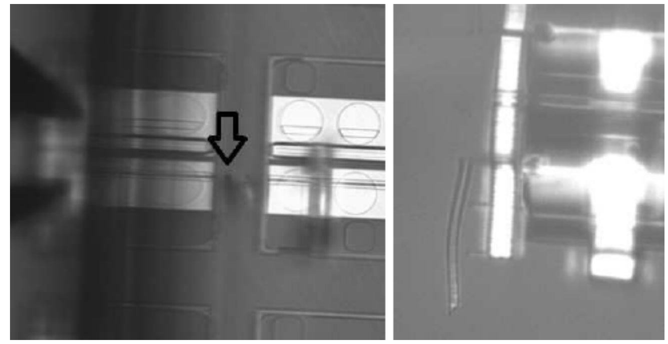

(a) (b)

Figure 11. (a) View through periscope probe aligned to facet of edge emitting laser supplied with current via DC-probes. (b) Side view of crashed probe with vertical WG detached from studs.

emission that should be between $10\text{-}20\,\mathrm{mW}$, before it finally broke. Probably due to thermal degradation since heat can not dissipate from the small tip. This shows a proof of concept, however for further tests lower emission power have to be used.

IV. Conclusion and Outlook

We presented our current state in hybrid lithography processing polymeric optical RDL via UV-lithography and μ-mirrors via 2PP-DLW. We demonstrated that SU8 spacers allow for setting of a low, reproducible proximity gap with stick resin, improving patterning results and making batch processing more easy. Comparison of Hg-lamp and dual wavelength LED-source showed, that the second gives improved patterning results both for WG-cores and clad openings, especially with respect to sidewall roughness. Next step is to measure attenuation of those greatly improved core cross sections. Thereafter the full polymeric RDL has to be put together, with the main challenge being good alignment and homogeneity of core thickness on topographic bottom clad. However the latter can be solved by having a nearly full bottom clad with only the necessary openings.

For μ-mirror structuring we introduced a process flow for automatic resin characterization yielding the to our knowledge most detailed published processing window characterization on OrmoComp and IP-DIP. Comparison showed that IP-DIP is more feasible due to bigger processing window. Thereafter roughness characterization showed that also with coarse writing hatch of $500\,\mathrm{nm}$ below $50\,\mathrm{nm}$ roughness can be achieved, even if single lines are visible in SEM and tactile profilometry measurement. In the future we will optically characterize μ-mirrors made with those parameters, to see if impact on performance is as low as expected. Additionally we showed that adhesion of IP-DIP to polymeric RDL is very good and no issues for proposed interposer. Finally we applied this to so-called periscope probe, providing a solution for wafer level testing of edge emitting lasers.

ACKNOWLEDGMENT

This Work has been supported by Germany's Federal Ministry of Education and Research (BMBF) within the project VE-Silhouette. The authors would like to thank I. Sotiriou, M. Göhler and N. Gohla for their extensive processing work.

.

REFERENCES

[1] M.-J. Lu, S.-Y. Mu, C.-S. Cheng, and J. Chen, "Advanced packaging technologies for co-packaged optics," in *Proc. of IEEE 72nd Electronic Components and Technology Conf. (ECTC)*. San Diego, CA, USA: IEEE, 2022, pp. 38–42.

[2] B. Chou, B. M. Sawyer*, G. Lyu, E. Timurdugan, C. Minkenberg, A. J. Zilkie, and D. McCann, "Demonstration of fan-out silicon photonics module for next generation co-packaged optics(cpo) application," in *Proc. of IEEE 72nd Electronic Components and Technology Conf. (ECTC)*. San Diego, CA, USA: IEEE, 2022, pp. 394–402.

[3] S. B. N. Gourikutty, M. C. Jong, C. V. Kanna, D. S. W. Ho, S. W. Wei, S. L. P. Siang, J. Wu, T. G. Lim, R. Mandal, J. T.-Y. Liow, and S. B. 1, "A novel packaging platform for high-performance optical engines in hyperscale data center applications," in *Proc. of IEEE 72nd Electronic Components and Technology Conf. (ECTC)*. San Diego, CA, USA: IEEE, 2022, pp. 422–427.

[4] A. Janta-Polczynski and M. Robitaille, "Optical fiber pigtails integration in co-package," in *Proc. of IEEE 72nd Electronic Components and Technology Conf. (ECTC)*. San Diego, CA, USA: IEEE, 2022, pp. 410–422.

[5] Z. Zhang, D. Felipe, V. Katopodis, P. Groumas, C. Kouloumentas, H. Avramopoulos, J.-Y. Dupuy, A. Konczykowska, A. Dede, A. Beretta, A. Vannucci, G. Cangini, R. Dinu, D. Schmidt, M. Moehrle, P. Runge, J.-H. Choi, H.-G. Bach, N. Grote, N. Keil, and M. Schell, "Hybrid photonic integration on a polymer platform," *Photonics*, vol. 2, no. 3, pp. 1005–1026, 9 2015. [Online]. Available: http://www.mdpi.com/2304-6732/2/3/1005

[6] E. Bosman, G. V. Steenberge, A. Boersma, S. Wiegersma, P. Harmsma, M. Karppinen, T. Korhonen, B. J. Offrein, R. Dangel, A. Daly, M. Ortsiefer, J. Justice, B. Corbett, S. Dorrestein, and J. Duis, "Scalable electro-photonic integration concept based on polymer waveguides," in *Optical Interconnects XVI*, H. Schröder and R. T. Chen, Eds. SPIE, mar 2016.

[7] L. Ma, X. Xu, and Z. He, "Single-mode polymer waveguides and devices for high-speed on-board optical interconnect application," in *Optical Interconnects XIX*, H. Schröder and R. T. Chen, Eds. SPIE, mar 2019.

[8] T. Barwicz, A. Janta-Polczynski, S. Takenobu, K. Watanabe, R. Langlois, Y. Taira, K. Suematsu, H. Numata, B. Peng, S. Kamlapurkar, S. Engelmann, P. Fortier, and N. Boyer, "Advances in interfacing optical fibers to nanophotonic waveguides via mechanically compliant polymer waveguides," *IEEE Journal of Selected Topics in Quantum Electronics*, vol. 26, no. 2, pp. 1–12, mar 2020.

[9] M. Hiltunen, M. T. Harjanne, T. Vehmas, B. Wälchli, P. Heimala, and T. Aalto, "Polymer interposer for efficient light coupling into 3 µm silicon-on-insulator waveguides," in *Optical Interconnects XX*, H. Schröder and R. T. Chen, Eds. SPIE, feb 2020.

[10] D. Weyers, K. Nieweglowski, L. Lorenz, and K. Bock, "Analysis of polymeric singlemode waveguides for inter-system communication," in *2021 23rd European Microelectronics and Packaging Conference & Exhibition (EMPC)*. IEEE, sep 2021.

[11] D. Weyers, A. Mistry, K. Nieweglowski, and K. Bock, "Hybrid lithography approach for single mode polymeric waveguides and out-of-plane coupling mirrors," in *Proc. of IEEE 72nd Electronic Components and Technology Conf. (ECTC)*. San Diego, CA, USA: IEEE, 2022, pp. 1919–1926.

[12] D. Weyers, K. Nieweglowski, and K. Bock, "Advances in UV-lithographic patterning of multi-layer waveguide stack for single mode polymeric RDL," in *2022 IEEE 9th Electronics System-Integration Technology Conference (ESTC)*. IEEE, sep 2022.

[13] J. Fischer and M. Wegener, "Three-dimensional optical laser lithography beyond the diffraction limit," *Laser & Photonics Reviews*, vol. 7, no. 1, pp. 22–44, mar 2012.

[14] X. Zhou, Y. Hou, and J. Lin, "A review on the processing accuracy of two-photon polymerization," *AIP Advances*, vol. 5, no. 3, p. 030701, mar 2015.

[15] A. Mistry, D. Weyers, K. Nieweglowski, and K. Bock, "Out-of-plane mirrors for single-mode polymeric rdl using direct laser writing," in *Proc. of 9th Electronic System-Integration Technology Conference (ESTC)*. Sibiu, Romania: IEEE, 2022.

[16] P.-I. Dietrich, M. Blaicher, I. Reuter, M. Billah, T. Hoose, A. Hofmann, C. Caer, R. Dangel, B. Offrein, U. Troppenz, M. Moehrle, W. Freude, and C. Koos, "In situ 3d nanoprinting of free-form coupling elements for hybrid photonic integration," *Nature Photonics*, vol. 12, no. 4, pp. 241–247, mar 2018.